

Data-driven core collapse supernova multilateration with first neutrino events

Farrukh Azfar,¹ Jeff Tseng,¹ Marta Colomer Molla,² Kate Scholberg,³ Alec Habig,⁴ Segev BenZvi,⁵ Melih Kara,⁶ James Kneller,⁷ Jost Migenda,⁸ Dan Milisavljevic,⁹ and Evan O'Connor¹⁰

¹*Department of Physics, Oxford University, Oxford OX1 3RH United Kingdom*

²*Université Libre de Bruxelles, 1050 Bruxelles, Belgium*

³*Department of Physics, Duke University, Durham, North Carolina 27708, USA*

⁴*Department of Physics and Astronomy, University of Minnesota Duluth, Duluth, Minnesota 55812, USA*

⁵*Department of Physics and Astronomy, University of Rochester, Rochester, New York 14627, USA*

⁶*Institute for Astroparticle Physics, Karlsruhe Institute of Technology, 76021 Karlsruhe, Germany*

⁷*Department of Physics, North Carolina State University, Raleigh, North Carolina 27695, USA*

⁸*e-Research, King's College London, London, United Kingdom*

⁹*Department of Physics and Astronomy, Purdue University, West Lafayette, Indiana 47907, USA*

¹⁰*The Oskar Klein Centre, Department of Astronomy,*

Stockholm University, AlbaNova, SE-10691 Stockholm, Sweden

(Dated: October 17, 2024)

A Galactic core-collapse supernova (CCSN) is likely to be observed in neutrino detectors around the world minutes to hours before the electromagnetic radiation arrives. The SNEWS2.0 network of neutrino and dark matter detectors aims to use the relative arrival times of the neutrinos at the different experiments to point back to the supernova. One of the simplest methods to calculate the CCSN direction is to use the first neutrino events detected through the inverse beta decay (IBD) process, $\bar{\nu}_e p \rightarrow e^+ n$. We will consider neutrino detectors sensitive to IBD interactions with low backgrounds. The difference in signal arrival times between a large and a small detector will be biased, however, with the first event at the smaller detector, on average, arriving later than that at the larger detector. This bias can be mitigated by using these first events in a data-driven approach without recourse to simulations or models. In this article, we demonstrate this method and its uncertainty estimate using pairs of detectors of different sizes and with different supernova distances. Finally, we use this method to calculate probability skymaps using four detectors (Super-Kamiokande, JUNO, LVD, and SNO+) and show that the calculated probabilities yield appropriate confidence intervals. The resulting skymaps should be useful for the multi-messenger community to follow up on the SNEWS2.0 Galactic CCSN neutrino alert.

I. INTRODUCTION

The collapse of a massive star in the Milky Way is a unique opportunity rich with physics on topics spanning astrophysics, cosmology, and fundamental particle physics[1]. At the same time, it is an exceedingly rare phenomenon, with rates estimated to be around 1.63 ± 0.46 per century [2]. In order to take maximal advantage of the next Galactic core-collapse supernova (CCSN), the upgrade of the SuperNova Early Warning System (SNEWS2.0) [3] aims to utilize the burst of neutrinos, which precedes electromagnetic radiation by minutes to hours, to alert the world's observatories. The SNEWS2.0 network also aims to use the relative arrival times of the neutrino bursts at each detector to point back to the supernova and guide follow-up observations.

The idea of multilateration (or, informally, “triangulation”) using the neutrino arrival times has been explored by multiple authors [4–8]. One of the simplest methods is to use the first observed events to determine the time differences between detector observations. For this method to be effective, the background should be negligible, which is a reasonable assumption for many underground detectors on the approximately ten-second timescale of a supernova burst. In addition to its simplicity, the method has the added advantages of being fast as well as relatively independent of supernova models, and thus works

in almost all circumstances. It is expected, of course, that pointing accuracy will ultimately be dominated by neutrino-electron elastic scattering events in large detectors such as Super-Kamiokande [9] and DUNE [10], but simple multilateration through a combination of detectors can provide added quickness and robustness to the search for a multi-messenger counterpart.

In this article, we describe a refined first-event method which reduces the inherent bias due to comparing detectors with different event yields, along with a practical data-driven method for estimating directional uncertainty, which is critical for assigning confidence levels to different directions (Sec. II). Sec. III describes the very simple simulation setup used to evaluate the method's performance, and Sec. IV presents the results of that evaluation. We combine multiple detectors in Sec. V to make skymaps with confidence intervals, and discuss the results in Sec. VI.

II. FIRST-EVENT BIAS

We will focus on four geographically dispersed detectors which are primarily sensitive to the inverse beta decay (IBD) process, $\bar{\nu}_e p \rightarrow e^+ n$: Super-Kamiokande (SK, Japan) [11], JUNO (China) [12], LVD (Italy) [13], and SNO+ (Canada) [14]. The IBD channel possesses ad-

vantages of sensitivity to a single anti-neutrino flavor, a large interaction cross section, and accessibility in a number of operating and near-future water Cherenkov and liquid scintillator detectors. Moreover, in detectors which can tag the subsequent neutron capture on protons or, in the case of Super-Kamiokande, on gadolinium nuclei, non-IBD events can be reduced significantly; for this study we assume the background is negligible. We assume further that the neutrino event rates as a function of time observed in every detector differ in their overall normalization but are otherwise nearly identical in shape, *i.e.*, the neutrino events are well above trigger thresholds, and Earth-matter effects are negligible. Finally, we neglect the very small, relatively low energy flux of $\bar{\nu}_e$, indicative of late-stage nuclear burning, which is expected to precede core collapse [15–18].

Let t_j be the time of the j -th observed event at a single detector, with $j = 1, 2, \dots, N$. The probability density function (PDF) for observing the first event at time t_1 is the product of two probabilities: first, of observing zero events in the time interval $(-\infty, t_1)$ followed by a single event in $[t_1, t_1 + dt_1)$. The Poisson PDF of the first is simply $e^{-\mu(t_1)}$, where $\mu(t_1) = \int_{-\infty}^{t_1} R(t)dt$ and $R(t)$ is the event rate at time t , *i.e.*, the number of events in the interval $[t, t + dt)$. The PDF of the second is simply $R(t_1)$, leading to the first-event PDF [19]

$$p_1(t_1) = R(t_1)e^{-\mu(t_1)}.$$

The expectation value of the first event time is then

$$E(t_1) = \frac{\int_{-\infty}^{\infty} t p_1(t) dt}{\int_{-\infty}^{\infty} p_1(t) dt} = \frac{\int_{-\infty}^{\infty} t R(t) e^{-\mu(t)} dt}{\int_{-\infty}^{\infty} R(t) e^{-\mu(t)} dt}. \quad (1)$$

We now make a numerical estimate of this expectation value $E(t_1)$ using the observed event times t_j in the following manner: we treat the t_j as random variables which are independent (up to the fact that they are sorted), and we approximate the integrals in Eq. 1 in the style of a Monte Carlo integration:

$$\begin{aligned} \int_{-\infty}^{\infty} t R(t) e^{-\mu(t)} dt &\approx \sum_{j=1}^N t_j e^{-\mu(t_j)} \approx \sum_{j=1}^N t_j e^{-j} \\ \int_{-\infty}^{\infty} R(t) e^{-\mu(t)} dt &\approx \sum_{j=1}^N e^{-\mu(t_j)} \approx \sum_{j=1}^N e^{-j}. \end{aligned}$$

In effect, in the first approximation, we treat $R(t)$ in the integrand as a weight function, with larger values indicating a higher density of events. In the second relation, we approximate the cumulative distribution $\mu(t_j)$ with the number of events up to that time, which is simply j . The numerical estimate of $E(t_1)$, which we denote $\langle t_1 \rangle$, is thus

$$E(t_1) \approx \langle t_1 \rangle \equiv \frac{\sum_{j=1}^N t_j e^{-j}}{\sum_{j=1}^N e^{-j}}, \quad (2)$$

which is essentially a weighted average which emphasizes the early events and exponentially suppresses the later ones. Indeed, it is clear that one needs only the early events to calculate these sums to an appropriate precision. On the other hand, the approximations used above can introduce their own biases; for instance, it is easily shown that $\langle t_1 \rangle > t_1$ by construction, whereas the first event time could occur before or after the true expectation value $E(t_1)$. It can also be seen that the approximation $\mu(t_j) \approx j$ works best for early times if the rate rises quickly. Conversely, if the rate rises slowly, the approximation can introduce sizable relative deviations from $\mu(t_j)$. It is worth noting that there is good agreement between supernova modeling groups on the rapid rise of the $\bar{\nu}_e$ lightcurve at early times—the phase most relevant to this study [20, 21].

If we wish to use the events of a large detector to estimate $\langle t_1 \rangle$ for a smaller detector, we can rescale the larger detector's rate $R(t)$ by a constant factor $\alpha < 1$, such as

$$R'(t) = \alpha R(t).$$

In that case, the rescaled estimate corresponding to Eq. 2 becomes

$$E(t_1^\alpha) \approx \langle t_1^\alpha \rangle \equiv \frac{\sum_{j=1}^N t_j e^{-\alpha j}}{\sum_{j=1}^N e^{-\alpha j}}. \quad (3)$$

The difference between $\langle t_1 \rangle$ and $\langle t_1^\alpha \rangle$ is the estimated bias of the observed arrival time between two detectors of unequal size.

Compared to Eq. 2, the exponential suppression in Eq. 3 is smaller term by term, and thus can be seen as a weighted average farther into the time series. In fact, it can be proven (see App. A) that $\langle t_1^\alpha \rangle > \langle t_1 \rangle$ for $\alpha < 1$. It is also evident that when calculating $\langle t_1^\alpha \rangle$, one should increase the number of early events by a factor of α^{-1} in order to achieve a similar desired level of accuracy.

Consider two detectors A and B which receive the neutrino signal with a true lag τ between them. Experiment A observes N_A events, $\{t_1^A, \dots, t_{N_A}^A\}$, while experiment B receives $N_B = \alpha N_A$ events, $\{t_1^B, \dots, t_{N_B}^B\}$. We define the “de-biased lag” as

$$Z \equiv t_1^A - t_1^B - \langle t_1^A \rangle + \langle t_1^{\alpha A} \rangle, \quad (4)$$

where $\langle t_1^{\alpha A} \rangle$ indicates the rescaled estimate from Eq. 3, based on the event times from detector A . Crucially, $\langle t_1^A \rangle$ and $\langle t_1^{\alpha A} \rangle$ have no lag between them; the only difference in the expectation values is due to the relative yield α . The difference $\langle t_1^A \rangle - \langle t_1^{\alpha A} \rangle$ therefore represents the estimated bias in the first-event difference due only to the relative yields of the two detectors. The expectation value of Z is thus, ideally, the lag itself, and $Z - \tau$ the residual bias.

The expected uncertainty on Z is determined by noting that t_1^A and t_1^B are independent measurements and hence

$$\sigma_Z^2 = \sigma_{t_1^A}^2 + \sigma_{t_1^B}^2. \quad (5)$$

The variance in t_1^A requires estimating the expectation value, following Eq. 1,

$$E((t_1^A)^2) = \frac{\int_{-\infty}^{\infty} t^2 p_1(t) dt}{\int_{-\infty}^{\infty} p_1(t) dt} \approx \langle (t_1^A)^2 \rangle \equiv \frac{\sum_{j=1}^{N_A} (t_j^A)^2 e^{-j}}{\sum_{j=1}^{N_A} e^{-j}}.$$

The variance in t_1^B , which is invariant with respect to the lag, can be evaluated using the data of detector B , or rescaling the data of detector A :

$$\begin{aligned} E((t_1^B - \langle t_1^B \rangle)^2) &\approx \langle (t_1^B)^2 \rangle - \langle t_1^B \rangle^2 \\ &\approx \langle (t_1^{\alpha A})^2 \rangle - \langle t_1^{\alpha A} \rangle^2. \end{aligned}$$

In practice, since the events in both detectors are subject to statistical fluctuations, we evaluate the expectation value with both datasets, and take the larger variance as a conservative estimate of $\sigma_{t_1^B}^2$.

It is possible, though it will not be implemented for the studies in this article, to derive a similar technique to estimate $E(t_1^\alpha)$ from data which is binned in time, and may include significant background levels. For instance, consider data from experiment A reported as M event counts n_k in time windows $[T_k, T_{k+1})$, with an estimated background b_k in each bin. The time windows do not have to be uniform in length, but they should be long enough such that $n_k - b_k > 0$. Eq. 2 then becomes

$$E(t_1) \approx \langle t_1^\alpha \rangle = \frac{\sum_{k=1}^M (n_k - b_k) T_k e^{-\alpha \mu_k}}{\sum_{k=1}^M (n_k - b_k) e^{-\alpha \mu_k}}. \quad (6)$$

where

$$\mu_k = \sum_{r=1}^{k-1} (n_r - b_r)$$

is the background-subtracted sum of event counts before time T_k . Similar expressions can be obtained to provide an estimate of the variance. In this way, neutrino telescopes such as IceCube [22, 23] and KM3NeT [24], which have large IBD signal yields but also large backgrounds and cannot identify CCSN neutrino events individually, can be incorporated directly into this supernova multi-lateration technique. In fact, it is expected that IceCube and KM3NeT will fit their data to determine the start of their neutrino bursts, and will report those times along with their own estimates of the uncertainty, as reported in [25, 26].

III. SIMULATION

We test our method using IBD lightcurves generated using the `Bollig_2016` [27] models of SNEWPY [28, 29], assuming a progenitor with $27M_\odot$ and the LS220 equation of state [30]. We also present results using a $11.2M_\odot$ progenitor mass for test purposes.

For all the Monte Carlo trials in this paper we use the same, but otherwise arbitrary, benchmark supernova

Detector 1	Detector 2	True lag (ms)
Super-Kamiokande	JUNO	-1.97
Super-Kamiokande	LVD	-25.15
Super-Kamiokande	SNO+	-14.66
JUNO	LVD	-23.17
JUNO	SNO+	-12.69
LVD	SNO+	10.48

TABLE I. True lag times (τ) for the neutrino bursts between pairs of detectors, for the simulated supernova.

Detector	$27M_\odot$ yield	$11.2M_\odot$ yield
Super-Kamiokande	7800	4000
JUNO	7200	3800
LVD	360	190
SNO+	280	150

TABLE II. Average IBD event yields assuming a distance of 10 kpc, adiabatic MSW oscillations, and normal neutrino mass ordering, from [3].

time (1 Nov 2021 at 05:22:36.328 GMT) and direction (300° right ascension and -30° declination). The four detectors are modelled using SNOwGLoBES[31] assuming a distance of 10 kpc, adiabatic MSW oscillations, and normal neutrino mass ordering. The true lag times among the detectors are given in Table I.

IV. RESULTS

We run 10000 Monte Carlo trials, each including generated IBD events with average yields given in Table II, following [3]. Fig. 1 shows the comparison between the observed first-event time differences, $t_1^A - t_1^B$, before any bias correction, and the true lag τ , for all pair combinations of the four detectors. As expected, experiments with similar yields (Super-Kamiokande with JUNO and LVD with SNO+) are centered close to zero, indicating small bias, while pairings of large detectors with small detectors exhibit significant bias. The distributions tend to peak on the negative side, because we have taken detector A always to be the larger one, which on average observes the first event earlier.

After estimating and correcting for the bias, the distributions of the de-biased lag minus the true time difference, $Z - \tau$, are shown in Fig. 2. As $Z - \tau$ is the difference between the de-biased lag and the true lag, it should ideally be zero. Indeed, the distributions over the Monte Carlo trials are seen to be largely symmetric and centered close to zero, though a negative tail is evident in pairings with smaller detectors. The widths of the distributions of $Z - \tau$ are listed in Table III, and are all narrower (though in the case of Super-Kamiokande and JUNO, just slightly) than the corresponding $t_1^A - t_1^B - \tau$ distributions.

Fig. 3 shows the mean residual bias, *i.e.*, the mean of the $Z - \tau$ distribution, as a function of the second experi-

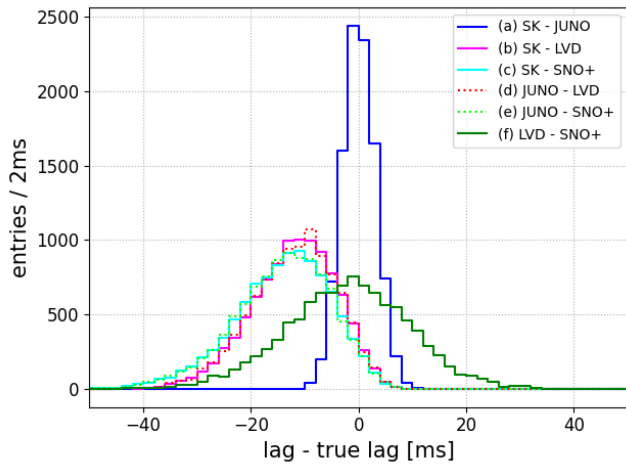


FIG. 1. Before bias correction: distributions of first-event time differences (observed lags) less true lags, $t_1^A - t_1^B - \tau$, over 10000 trials with the $27M_\odot$ IBD lightcurve shape at 10 kpc. Pairwise differences are always computed such that detector A is larger.

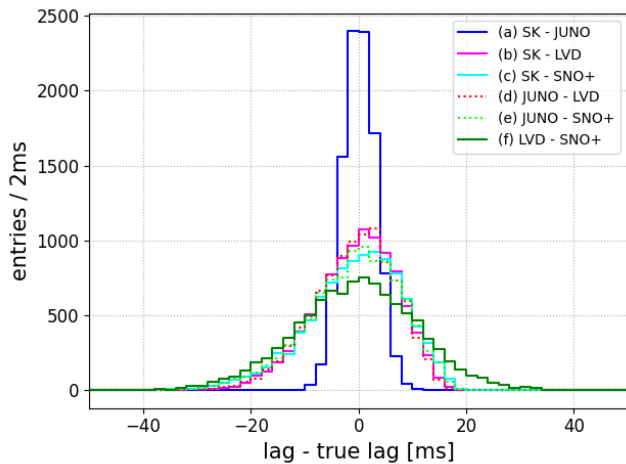


FIG. 2. After bias correction: residual bias (de-biased lag less true lag, $Z - \tau$) distributions over 10000 trials with the $27M_\odot$ IBD lightcurve shape at 10 kpc.

ment yield, where the first detector (Super-Kamiokande) is held at an average yield of 7800 events. The behavior of the mean residual bias is largely uniform across different detector locations, and therefore across true lag values. Even with the smallest detector, SNO+, expecting 280 events at 10 kpc from the chosen model, the residual bias is less than 1 ms. As the yields become more symmetric, one expects the residual bias to approach zero, but in fact it approaches +0.2 ms, a result of the rising $\bar{\nu}_e$ energy at early times coupled with the higher energy threshold for detecting IBD events in Super-Kamiokande, the sole water detector among the four simulated. The mean observed RMS decreases from $O(10)$ ms to a minimum variability around $O(3)$ ms with increasing yield. For

Detector 1	Detector 2	RMS (ms)
Super-Kamiokande	JUNO	3.1
Super-Kamiokande	LVD	7.7
Super-Kamiokande	SNO+	8.9
JUNO	LVD	7.7
JUNO	SNO+	8.9
LVD	SNO+	11.3

TABLE III. Observed RMS widths of the distributions of $Z - \tau$, with the $27M_\odot$ IBD lightcurve shape at 10 kpc.

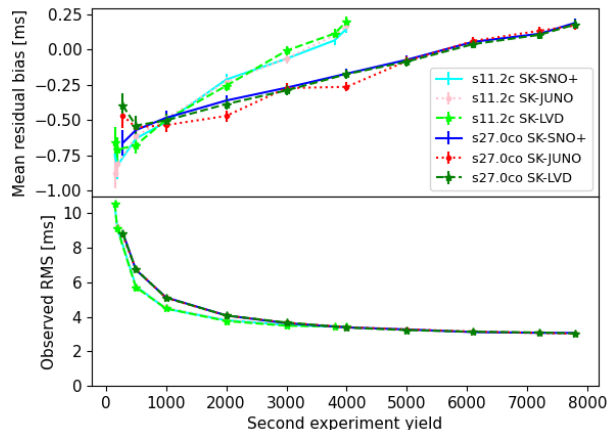


FIG. 3. Top: mean residual bias for Super-Kamiokande compared with detector locations at JUNO (red), LVD (green), and SNO+ (blue) over 10000 trials of the IBD lightcurve shape for $27M_\odot$, where the average Super-Kamiokande yield is held constant at 7800 events. Also shown are mean residual biases for the $11.2M_\odot$ lightcurve, with the Super-Kamiokande average yield held at 4000 events, and the yield is varied for JUNO (pink), LVD (lime green), and SNO+ (cyan) locations. Bottom: mean observed RMS over 10000 trials.

all yields, the residual bias is much smaller than the observed RMS, which reflects the measurement uncertainty for any single trial (or supernova event).

Mean residual biases and mean observed RMS's are also shown for the $11.2M_\odot$ model, again with the LS220 equation of state. As with the $27M_\odot$ model, the mean bias remains below 1 ms, and the mean RMS decreases from $O(10)$ ms to around $O(3)$ ms.

Fig. 4 compares the observed RMS with the estimated uncertainty calculated using Eq. 5. The relationship between the observed and expected values is mostly linear, though saturating for large yields at 2.6 ms for the mean of the expected uncertainties, and about 3.1 ms for the corresponding observed RMS. The fact that the calculated uncertainty differs from the observed variability is not surprising given the approximations used. In simplified numerical cases, replacing $\mu(t_j)$ with j by itself can be shown to account for differences of a similar size. In order to draw reasonable confidence intervals from the data of a single supernova, in the following we will use the estimated uncertainty and multiply it by a “fudge fac-

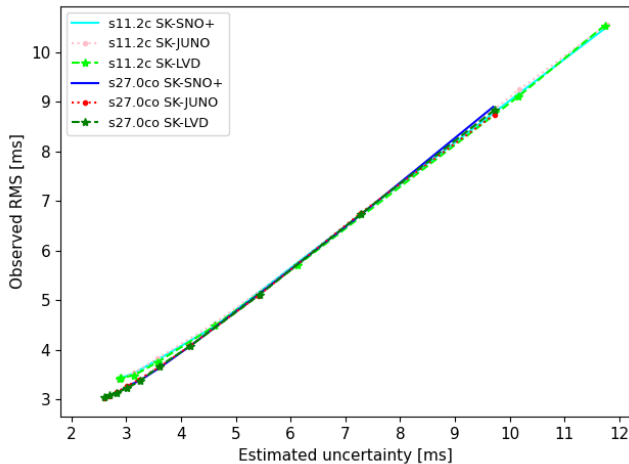


FIG. 4. Mean observed RMS as a function of the mean estimated uncertainty from Eq. 5 for the IBD lightcurve shape. Color scheme is the same as that of Fig. 3.

tor” of 1.2 (the ratio between the expected and observed RMS values), even though this straightforward inflation generally overestimates the measurement uncertainty at lower yields (see Sec. V).

We then run Monte Carlo trials with the supernova at different distances, from 6 to 20 kpc, scaling the nominal event yields accordingly. The mean residual biases and mean observed RMS are shown as a function of supernova distance in Fig. 5. The biases and observed RMS grow with distance, as expected. This pattern changes, however, at 20 kpc. The reason is illustrated in Fig. 6: for pairings between a large and a small detector, the peak of the $Z - \tau$ distribution has shifted toward positive values, while a sizable negative tail has grown, in some cases pulling the mean back to small values. The shift is likely related to the asymmetry in the approximation noted after Eq. 2: for a pair of detectors with similar yields, such as Super-Kamiokande and JUNO, the asymmetries largely cancel out in the difference in Z . Lower yields, on the other hand, exacerbate the asymmetry, and their effects do not cancel when detectors of very different yields are paired. Indeed, the peaks of those pairings all appear on the positive side, indicating an over correction of the bias.

V. POINTING

We combine the time differences into a direction by calculating the χ^2 between the observed time differences (with bias correction) and the predicted time differences for different supernova directions. We use the centers of the HEALPix [32][33] pixels as the test directions, and assign the χ^2 for that direction to each pixel. We also inflate the uncertainty estimates by a factor 1.2, as suggested in Sec. IV, and subtract the minimum χ^2

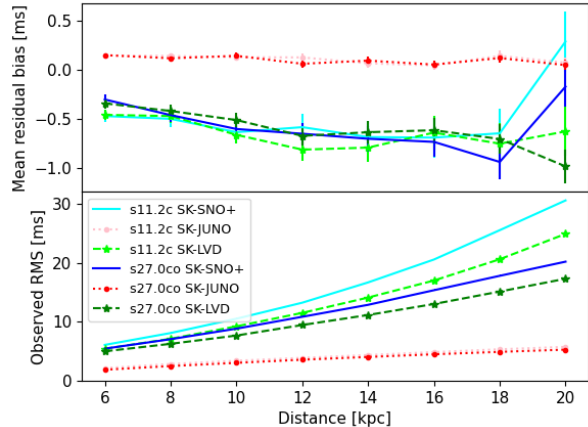


FIG. 5. Mean residual bias and mean observed RMS using the IBD shape, but at different distances. The color scheme used is the same as that of Fig. 3.

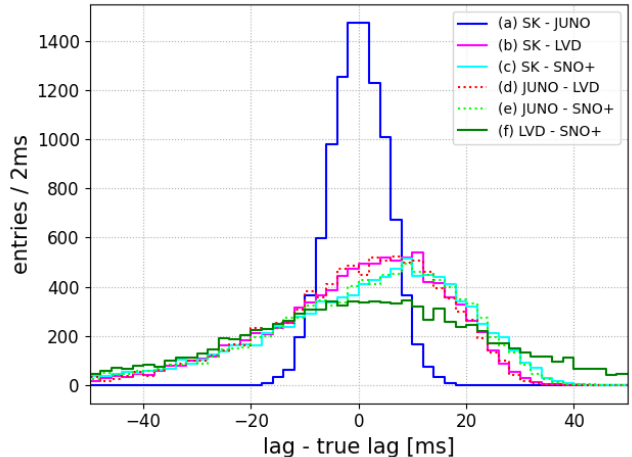


FIG. 6. Residual bias distributions over 10000 trials with the $27M_{\odot}$ IBD lightcurve shape, but at 20 kpc distance.

value from that of all the pixels. The resulting probability skymaps, with HEALPix $N_{side} = 8$, are shown in Fig. 7 for three CCSN explosions simulated with the $27M_{\odot}$ model at a distance of 10 kpc.

One way to test the coverage is to count the number of times, among the 10000 trials, any given pixel is deemed most likely, *i.e.*, has the minimum χ^2 . The resulting skymap, shown in Fig. 8, resembles the individual probability maps in shape and extent.

A more rigorous test of the coverage can be performed by calculating the confidence interval to which the true direction has been assigned. For this purpose, we plot the value of the χ^2 cumulative probability distribution function for the χ^2 for the pixel containing the true direction. The result is shown in Fig. 9. Ideally, this histogram would be flat, with (for instance) 40% of the histogram

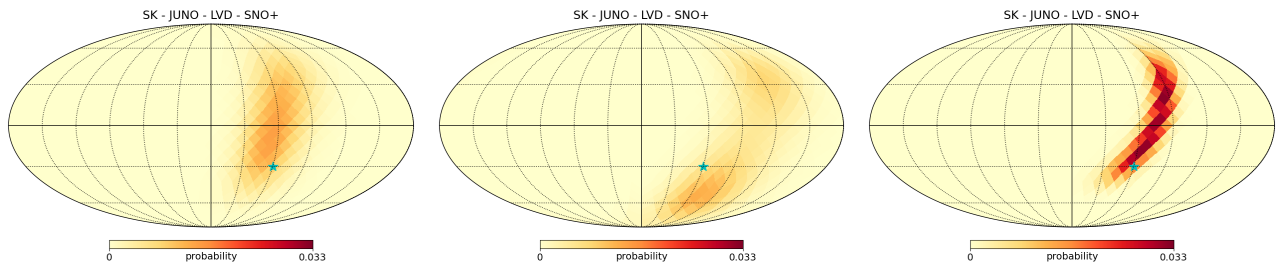


FIG. 7. Sample probability skymaps for three different Monte Carlo trials combining the four detectors. The true location for all the trials is indicated with the light blue star.

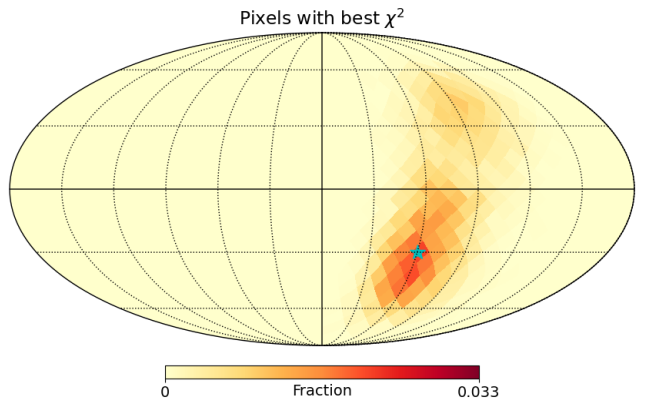


FIG. 8. Skymap built with pixels of maximum probability over 10000 trials. The true location is indicated with the light blue star.

below the value 0.4, *i.e.*, with the true position lying within the 40% region 40% of the time. Instead, there is a small spike at 1 and a slow rise to toward lower values, indicating that uncertainties have been over-estimated on average, with 45% of the histogram below 0.4. The spike in the lowest bin is an artifact of the pixellation, since the true direction does not lie at the center of the pixel, leading to a number of trials for which the χ^2 difference evaluates artificially close to zero. If the resolution of the skymap is increased, the spike in the lowest bin disappears.

VI. DISCUSSION

In this article, we have further developed the first-event method by deriving a data-driven approach for reducing the time difference bias due to two detectors' differing event yields. The time delay between the first IBD events in different detectors, along with its estimated uncertainty, have then been used for the purpose of localizing the supernova via multilateration. The method has been tested in Monte Carlo trials with the `Bollig_2016` models in SNEWPY. The residual bias is reduced to less than 1 ms even when two detectors differ in size by more

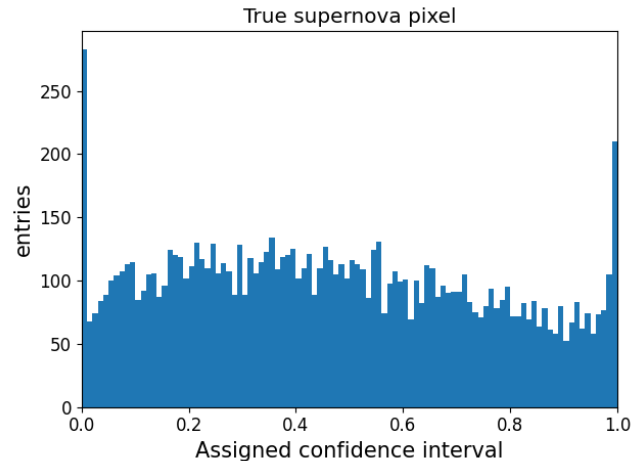


FIG. 9. Confidence interval assigned to the pixel of the true supernova direction.

than an order of magnitude. We have also demonstrated how the uncertainty can be estimated directly from the data, and that the resulting probability skymaps resemble those generated from Monte Carlo trials. The method is suitable for real-time use in SNEWS2.0.

The main assumptions in this method are (i) that background can be neglected in the contributing detectors over the supernova burst timescale, (ii) that the shape of the time profile of the event rate is similar for all of them, and (iii) that the early part of the event rate shape is characterized by a single, rapid rise. These assumptions are reasonable for coincidence-tagged IBD events in at least several large underground water Cherenkov and liquid scintillator detectors. Where the background level is high, as in neutrino telescopes like IceCube and KM3NeT, the assumption of a single rapid rise may still lead to a well-defined starting time similar to the expected first event time $\langle t_1 \rangle$, such that after background subtraction a useful time difference can be integrated into first-event multilateration. A formula for using binned data with large backgrounds has also been derived (Eq. 6). It should be noted that the burst starting time used here is *not* the same as the bounce time, since calculating the latter requires more sophisticated model-

based assumptions.

It is expected that SNEWS2.0 will employ multiple algorithms to multilaterate the supernova direction under different assumptions and levels of model dependence. At least some methods should minimize model dependence, as the present method does. Moreover, the first-event method can also be used as an initial direction which can be refined by slower but more precise methods that utilize features of the entire lightcurve. For instance, algorithms using more information about the lightcurve can take advantage of distinctive features that may occur later in the supernova, such as the rapid flux decrease due to the formation of a black hole $O(1)$ second after the initial bounce [6, 34, 35]. In this way, the global multi-messenger community can increase the chance to take full advantage of one of the most brilliant events in the

galaxy.

VII. ACKNOWLEDGEMENTS

FA and JT acknowledge support from the Science and Technology Facilities Council (STFC), United Kingdom. MCM acknowledges the support of the Belgian Fund for Scientific Research, the FRS-FNRS (Fond pour la Recherche Scientifique). KS, AH, and SB acknowledge NSF support from grant PHY-2209534, JPK from grant PHY-2209449, and DM from grants PHY-2209451 and AST-2206532. EO is supported by the Swedish Research Council (Project No. 2020-00452). Plots were generated with matplotlib [36], and some results derived using the healpy [37] and HEALPix packages.

-
- [1] See, for instance, [38–40], and recent articles such as [41–43].
- [2] K. Rozwadowska, F. Vissani, and E. Cappellaro, On the rate of core collapse supernovae in the milky way, *New Astron.* **83**, 101498 (2021), arXiv:2009.03438 [astro-ph.HE].
- [3] S. Al Kharusi *et al.* (SNEWS), SNEWS 2.0: a next-generation supernova early warning system for multi-messenger astronomy, *New J. Phys.* **23**, 031201 (2021), arXiv:2011.00035 [astro-ph.HE].
- [4] J. F. Beacom and P. Vogel, Can a supernova be located by its neutrinos?, *Phys. Rev. D* **60**, 033007 (1999), arXiv:astro-ph/9811350.
- [5] T. Mühlbeier, H. Nunokawa, and R. Zukanovich Funchal, Revisiting the Triangulation Method for Pointing to Supernova and Failed Supernova with Neutrinos, *Phys. Rev. D* **88**, 085010 (2013), arXiv:1304.5006 [astro-ph.HE].
- [6] V. Brdar, M. Lindner, and X.-J. Xu, Neutrino astronomy with supernova neutrinos, *JCAP* **04**, 025, arXiv:1802.02577 [hep-ph].
- [7] N. B. Linzer and K. Scholberg, Triangulation Pointing to Core-Collapse Supernovae with Next-Generation Neutrino Detectors, *Phys. Rev. D* **100**, 103005 (2019), arXiv:1909.03151 [astro-ph.IM].
- [8] A. Coleiro, M. Colomer Molla, D. Dornic, M. Lincetto, and V. Kulikovskiy, Combining neutrino experimental light-curves for pointing to the next galactic core-collapse supernova, *Eur. Phys. J. C* **80**, 856 (2020), arXiv:2003.04864 [astro-ph.HE].
- [9] Y. Kashiwagi *et al.* (Super-Kamiokande), Performance of SK-Gd's Upgraded Real-time Supernova Monitoring System (2024), arXiv:2403.06760 [astro-ph.HE].
- [10] A. Abed Abud *et al.* (DUNE), Supernova Pointing Capabilities of DUNE (2024), arXiv:2407.10339 [hep-ex].
- [11] Y. Fukuda *et al.* (Super-Kamiokande), The Super-Kamiokande detector, *Nucl. Instrum. Meth. A* **501**, 418 (2003).
- [12] A. Abusleme *et al.* (JUNO), JUNO physics and detector, *Prog. Part. Nucl. Phys.* **123**, 103927 (2022), arXiv:2104.02565 [hep-ex].
- [13] M. Aglietta *et al.*, The Most powerful scintillator supernovae detector: LVD, *Nuovo Cim. A* **105**, 1793 (1992).
- [14] V. Albanese *et al.* (SNO+), The SNO+ experiment, *JINST* **16** (08), P08059, arXiv:2104.11687 [physics.ins-det].
- [15] A. Odrzywolek, M. Misiaszek, and M. Kutschera, Detection possibility of the pair - annihilation neutrinos from the neutrino - cooled pre-supernova star, *Astropart. Phys.* **21**, 303 (2004), arXiv:astro-ph/0311012.
- [16] A. Odrzywolek, M. Misiaszek, and M. Kutschera, Neutrinos from pre-supernova star, *Acta Phys. Polon. B* **35**, 1981 (2004), arXiv:astro-ph/0405006.
- [17] K. M. Patton, C. Lunardini, and R. J. Farmer, Presupernova neutrinos: realistic emissivities from stellar evolution, *Astrophys. J.* **840**, 2 (2017), arXiv:1511.02820 [astro-ph.SR].
- [18] K. M. Patton, C. Lunardini, R. J. Farmer, and F. X. Timmes, Neutrinos from beta processes in a presupernova: probing the isotopic evolution of a massive star, *Astrophys. J.* **851**, 6 (2017), arXiv:1709.01877 [astro-ph.HE].
- [19] V. Brdar and X.-J. Xu, Timing and multi-channel: novel method for determining the neutrino mass ordering from supernovae, *JCAP* **08**, 067, arXiv:2204.13135 [hep-ph].
- [20] E. O'Connor *et al.*, Global Comparison of Core-Collapse Supernova Simulations in Spherical Symmetry, *J. Phys. G* **45**, 104001 (2018), arXiv:1806.04175 [astro-ph.HE].
- [21] R. M. Cabezón, K.-C. Pan, M. Liebendörfer, T. Kuroda, K. Ebinger, O. Heinemann, F.-K. Thielemann, and A. Perego, Core-collapse supernovae in the hall of mirrors. A three-dimensional code-comparison project, *Astrophys. J.* **619**, A118 (2018), arXiv:1806.09184 [astro-ph.HE].
- [22] M. G. Aartsen *et al.* (IceCube), The IceCube Neutrino Observatory: Instrumentation and Online Systems, *JINST* **12** (03), P03012, arXiv:1612.05093 [astro-ph.IM].
- [23] R. Abbasi *et al.* (IceCube), An End-to-End Test of the Sensitivity of IceCube to the Neutrino Burst from a Core-Collapse Supernova, *PoS ICRC2021*, 1085 (2021), arXiv:2107.08098 [astro-ph.HE].
- [24] S. Adrian-Martinez *et al.* (KM3Net), Letter of intent for KM3NeT 2.0, *J. Phys. G* **43**, 084001 (2016),

- arXiv:1601.07459 [astro-ph.IM].
- [25] R. Cross, A. Fritz, and S. Griswold (IceCube), Eleven Year Search for Supernovae with the IceCube Neutrino Observatory, PoS **ICRC2019**, 889 (2020), arXiv:1908.07249 [astro-ph.HE].
- [26] S. Aiello *et al.* (KM3NeT), The KM3NeT potential for the next core-collapse supernova observation with neutrinos, Eur. Phys. J. C **81**, 445 (2021), arXiv:2102.05977 [astro-ph.HE].
- [27] A. Mirizzi, I. Tamborra, H.-T. Janka, N. Saviano, K. Scholberg, R. Bollig, L. Hudepohl, and S. Chakraborty, Supernova Neutrinos: Production, Oscillations and Detection (2016), arXiv:1508.00785 [astro-ph.HE].
- [28] A. L. Baxter, S. BenZvi, J. C. Jaimes, A. Coleiro, M. C. Molla, D. Dornic, T. Goldhagen, A. Graf, S. Griswold, A. Habig, R. Hill, S. Horiuchi, J. P. Kneller, R. F. Lang, M. Lincetto, J. Migenda, K. Nakamura, E. O'Connor, A. Renshaw, K. Scholberg, C. Tunnell, N. Uberoi, A. Worlikar, and T. S. Collaboration, Snewpy: A data pipeline from supernova simulations to neutrino signals, The Astrophysical Journal **925**, 107 (2022).
- [29] A. L. Baxter, S. BenZvi, J. C. Jaimes, A. Coleiro, M. C. Molla, D. Dornic, S. Griswold, T. Goldhagen, A. Graf, A. Habig, R. Hill, S. Horiuchi, J. P. Kneller, M. Lamoureux, R. F. Lang, M. Lincetto, J. Migenda, M. Myers, E. O'Connor, A. Renshaw, K. Scholberg, A. Sheshukov, J. Tseng, C. Tunnell, N. Uberoi, and A. Worlikar, Snewpy: A data pipeline from supernova simulations to neutrino signals, Journal of Open Source Software **6**, 3772 (2021).
- [30] S. E. Woosley and A. Heger, Nucleosynthesis and Remnants in Massive Stars of Solar Metallicity, Phys. Rept. **442**, 269 (2007), arXiv:astro-ph/0702176.
- [31] A. Beck *et al.*, <https://github.com/SNOwGLoBES/snowglobes>, 2016.
- [32] K. M. Górski, E. Hivon, A. J. Banday, B. D. Wandelt, F. K. Hansen, M. Reinecke, and M. Bartelmann, HEALPix: A Framework for High-Resolution Discretization and Fast Analysis of Data Distributed on the Sphere, Astrophys. J. **622**, 759 (2005), arXiv:astro-ph/0409513 [astro-ph].
- [33] <http://healpix.sf.net/>.
- [34] J.-S. Wang, J. Tseng, S. Gullin, and E. P. O'Connor, Nonradial neutrino emission upon black hole formation in core collapse supernovae, Phys. Rev. D **104**, 104030 (2021), arXiv:2109.11430 [astro-ph.HE].
- [35] S. Gullin, E. P. O'Connor, J.-S. Wang, and J. Tseng, Neutrino Echos following Black Hole Formation in Core-collapse Supernovae, Astrophys. J. **926**, 212 (2022), arXiv:2109.13242 [astro-ph.HE].
- [36] J. D. Hunter, Matplotlib: A 2d graphics environment, Computing in Science & Engineering **9**, 90 (2007).
- [37] A. Zonca, L. Singer, D. Lenz, M. Reinecke, C. Rosset, E. Hivon, and K. Gorski, healpy: equal area pixelization and spherical harmonics transforms for data on the sphere in python, Journal of Open Source Software **4**, 1298 (2019).
- [38] Y. Koshio, G. D. O. Gann, E. O'Sullivan, and I. Tamborra, Snowmass 2021 topical group report: Neutrinos from natural sources (2022), arXiv:2209.04298 [hep-ph].
- [39] S. Furusawa and H. Nagakura, Nuclei in core-collapse supernovae engine, Prog. Part. Nucl. Phys. **129**, 104018 (2023), arXiv:2211.01050 [nucl-th].
- [40] A. Arcones *et al.*, White paper on nuclear astrophysics and low energy nuclear physics Part 1: Nuclear astrophysics, Prog. Part. Nucl. Phys. **94**, 1 (2017), arXiv:1603.02213 [astro-ph.SR].
- [41] L. Visinelli, T. T. Yanagida, and M. Zantedeschi, Do neutrinos bend? consequences of an ultralight gauge field as dark matter (2024), arXiv:2407.18300 [hep-ph].
- [42] A. Lella, E. Ravensburg, P. Carena, and M. C. D. Marsh, Supernova limits on 'qcd axion-like particles' (2024), arXiv:2405.00153 [hep-ph].
- [43] C. Li, Z. Liu, W. Lu, and Z. Ye, Low-energy supernova constraints on millicharged particles (2024), arXiv:2408.04953 [hep-ph].

Appendix A: First event times for smaller experiments

We can see that $\langle t_1^\alpha \rangle > \langle t_1 \rangle$ for all $\alpha < 1$ by differentiating with respect to α as α decreases. We start from the difference formula

$$-\frac{d\langle t_1^\alpha \rangle}{d\alpha} = \lim_{\epsilon \rightarrow 0} \frac{\langle t_1^{\alpha-\epsilon} \rangle - \langle t_1 \rangle^\alpha}{\epsilon}. \quad (\text{A1})$$

The numerator is

$$\frac{\sum_{j=1}^N t_j e^{-(\alpha-\epsilon)j}}{\sum_{j=1}^N e^{-(\alpha-\epsilon)j}} - \frac{\sum_{j=1}^N t_j e^{-\alpha j}}{\sum_{j=1}^N e^{-\alpha j}}$$

which to first order in ϵ (higher orders vanishing in the limit) is

$$\frac{(\sum_j t_j j e^{-\alpha j})(\sum_k e^{-\alpha k}) - (\sum_j t_j e^{-\alpha j})(\sum_k k e^{-\alpha k})}{(\sum_j e^{-\alpha j})^2}.$$

The denominator is always positive, so we concentrate on the numerator, which becomes

$$\sum_{j=1}^N \sum_{k=1}^N t_j (j-k) e^{-\alpha(j+k)} = \sum_{j=1}^N \sum_{k=1}^N t_j w_{jk} \quad (\text{A2})$$

where $w_{jk} \equiv (j-k)e^{-\alpha(j+k)}$. It is easy to see that w_{jk} is antisymmetric in its indices and $w_{jk} > 0$ whenever $j > k$. We split the sum into lower and upper triangular regions in (j, k)

$$\sum_{j=1}^N \sum_{k=1}^{j-1} t_j w_{jk} + \sum_{j=1}^N \sum_{k=j+1}^N t_j w_{jk}.$$

The terms in the second double sum can be reordered before swapping the dummy indices:

$$\begin{aligned} \sum_{j=1}^N \sum_{k=j+1}^N t_j w_{jk} &= \sum_{k=1}^N \sum_{j=1}^{k-1} t_j w_{jk} \\ &= \sum_{j=1}^N \sum_{k=1}^{j-1} t_k w_{kj} \\ &= - \sum_{j=1}^N \sum_{k=1}^{j-1} t_k w_{jk} \end{aligned}$$

The expression in Eq. A2 is now

$$\sum_{j=1}^N \sum_{k=1}^N t_j w_{jk} = \sum_{j=1}^N \sum_{k=1}^{j-1} (t_j - t_k) w_{jk}.$$

We know that since $j > k$ for all terms in the sum, $w_{jk} > 0$. Moreover, $t_j - t_k > 0$ because the event times

are ordered in increasing time. The expression in Eq. A1 thus is positive, and $\langle t_1^\alpha \rangle$ increases monotonically, as α decreases. It is thus shown that when using a single dataset to estimate the expectation values of the first event time at smaller experiments, that expectation value trends later as the experiment gets smaller, as one would expect.